Investigating the structural stability and electronic properties of carbon doped silicon anode for lithium-ion batteries.

Samson Singo[1]*, *Katlego* Phoshoko[2], *Tshidi* Mogashoa[1], *Phuti* Ngoepe[1] and *Raesibe* Ledwaba[1]

[1]Materials Modelling Centre, University of Limpopo, Private Bag x1106, Sovenga 0727, South Africa.
[2]Data Intensive Research Initiative of South Africa, Council for Scientific and Industrial Research, P.O. Box 395, Pretoria, 0001, South Africa.

Abstract. Silicon is an attractive anode material for lithium-ion batteries due to it having a high theoretical capacity of 4200 mAh/g, however, it experiences severe volume changes during the lithiation and delithiation processes. Doping with carbon can help to mitigate these severe volume changes and increase the electrochemical performance, since carbon forms strong covalent bonds with silicon which are difficult to break as such it acts as a mechanical buffer to accommodate volume expansion hence maintain structural integrity. Furthermore, it forms continuous pathways for electron transport. In this study, the cluster expansion technique was successfully used to generate a silicon carbide (SiC_2) structure, which has a hexagonal symmetry and is thermodynamically stable. The density of states and band structure of SiC_2 illustrated metallic behaviour, thus promoting conductivity.

1 Introduction

Lithium-ion batteries (LIBs) serve as versatile energy storage systems which can be cycled by charging and discharging processes, they have low self-discharge rate and high energy density [1]. Currently, LIBs are widely used in portable electronic devices, aerospace equipment and electrical vehicles. Commercially, graphite is being used as an anode material for LIBs, but it is hindered by its low theoretical capacity (372 mAh/g) hence there is a need for a new anode material of which silicon has shown to be a viable alternative owing to its high theoretical capacity (4200 mAh/g) [2-3]. Silicon is hindered by the severe volume change that leads to the loss of electrical contact and excessive formation of the solid electrolyte interphase leading to a limited cycle life and reduced coulombic efficiency [4].

Various attempts have been made to address these issues by modifying silicon using methods such as nanotechnology [5] and designing nanostructures [6]. However, these approaches improved performance as compared to pure silicon, they do not fully resolve these challenges. Another promising strategy designed to mitigate these challenges is the

* Corresponding author: smsnsingo@gmail.com

incorporation of carbon into the silicon structure, forming a carbon-doped silicon composite. This combination helps maintain structural integrity and improves electrical conductivity, facilitates better electron transfer and enhances rate capability. Additionally, the formation of a stable solid electrolyte interface on the silicon surface protects it from degradation while allowing efficient lithium transport, thus further improving cycling stability [7-8].

This study employs computational methods to investigate the effects of carbon doping in silicon, with the intent being to enhance the structural stability and improve the conductivity of silicon, thus boosting the performance of LIBs.

2 Methodology

This work applied the cluster expansion approach to explore new carbon-doped silicon phases, with the cross-validation score serving as a measure of the predictive accuracy [9]. Structural and electronic properties of the predicted configurations were evaluated using density functional theory (DFT) within the Vienna Ab Initio Simulation Package (VASP), employing the generalized gradient approximation with the Perdew–Burke–Ernzerhof (GGA-PBE) functional [10–12]. Calculations were carried out with a plane-wave cut-off energy of 730 eV and a k-point mesh spacing of 0.121 1/Å in the Brillouin zone, generated via the Monkhorst–Pack scheme [13]. The reference silicon structure (Figure 1) is cubic, with lattice parameters a = b = c = 3.943 Å and was doped with carbon at the 4a Wyckoff site.

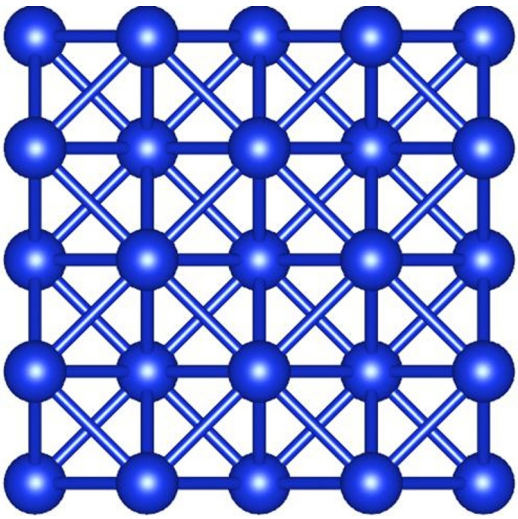

Fig. 1. Conventional unit of cell of silicon (Fm-3m) structure.

3 Results and discussion

3.1 Cluster expansion for Si-C alloy

The cluster expansion method was employed to predict the ground-state structures of carbon-doped silicon. Figure 2 depicts the iterative optimization process, highlighting both the number of iterations and the new structures generated at each stage. Over four iterations, the expansion produced eighteen new phases. By the final iteration, the model reached a cross-

validation score of 4.2 meV/atom which is well below the 5 meV/atom threshold demonstrating reliable predictive accuracy [14].

Figure 3 shows the binary ground-state diagram, which summarizes the predicted structures and their corresponding formation energies. In this diagram, green crosses denote the cluster expansion predicted heats of formation for training set structures, while green squares indicate their DFT-calculated counterparts. Grey crosses represent predicted formation energies of other structures generated by the expansion. The results reveal eighteen new phases, all situated within the miscibility gap and exhibiting negative heats of formation, indicating thermodynamic stability. Among these, the ce8 structure lies directly on the DFT ground-state line, making it the most stable configuration. When the symmetry of the structure was refined, it yielded a chemical formula of SiC_2, corresponding to 30% silicon and 70% carbon. This phase displays a remarkably low heat of formation (-2800 meV/site), far more stable than the parent phases, which have heats of formation of 0 meV/site.

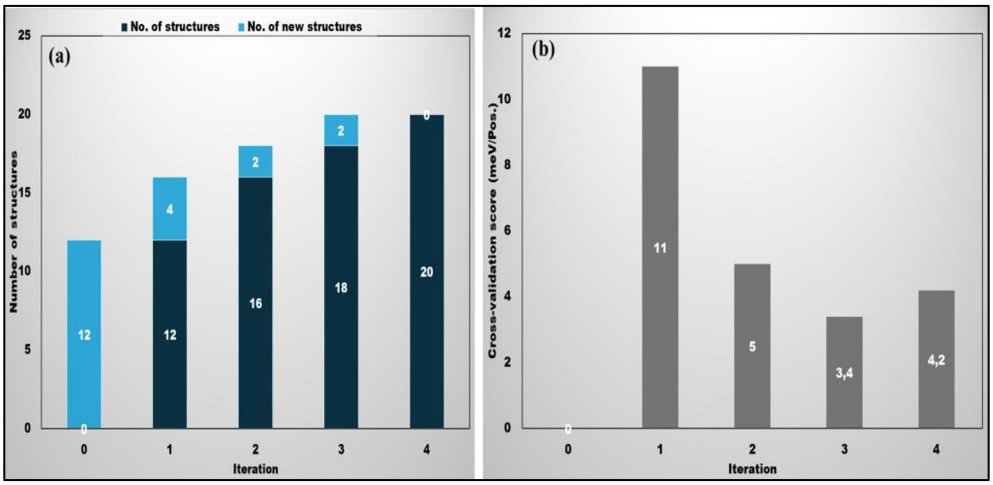

Fig. 2. Graphical representation of the (a) iterative optimization progress and (b) the cross-validation score per iteration of the Fm-3m based cluster expansion.

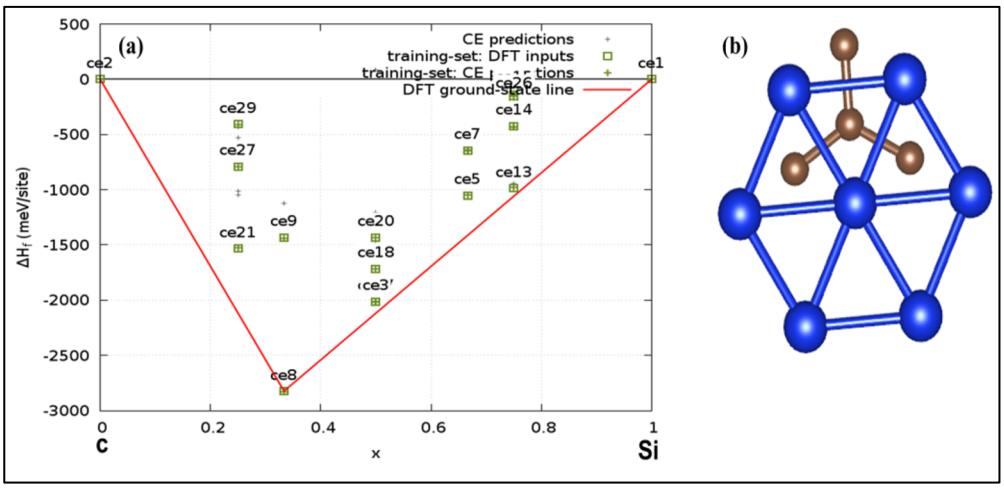

Fig. 3. (a) Binary ground state diagram of silicon doped with carbon and (b) The structure lying on the DFT ground-state line.

3.2 Structural properties

The lattice parameters of the silicon and carbon structures are in good agreement with the experimental values since their percentage difference is less than 5%. Moreover, both structures are cubic in symmetry as shown in table 1. The optimized SiC_2 Structure adopts a hexagonal crystal symmetry with a space group of P6/mmm, this symmetry suggests that the structure is layered. This structure was identified as the most thermodynamically stable phase among those generated during the cluster expansion simulation, as shown by having the lowest heat of formation (-2800 meV/site). The unit cells of the SiC_2 show that silicon atoms occupy high symmetry Wyckoff positions at (0, 0, 0), while carbon atoms are located at (0.333333, 0.666667, 0.5) forming planar arrangement around the silicon atoms. The small lattice parameters and cell volume of of SiC_2 indicate tighter atomic packing, leading to stronger interatomic interactions that enhance both structural and thermodynamic stability. Furthermore, the close positioning of the atoms can lead to electronic orbitals overlapping, which may increase the density of states.

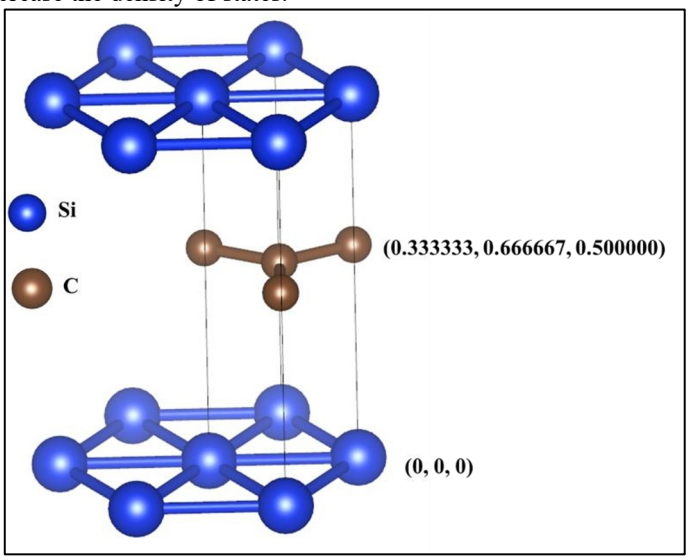

Fig. 4. Schematic crystal structure of SiC_2 in hexagonal form.

Table 1. Lattice parameters of the predicted structures and their parent lattice.

Structure	Space group	Lattice parameters (Å)			Angle (°)	
		a	b	c	α	γ
Si	Fm-3m	3.943 (3.820) [15]	3.943 (3.820) [15]	3.943 (3.820) [15]	90.0	90.0
C	Fm-3m	3.567 (3.570) [16]	3.567 (3.570) [16]	3.567 (3.570) [16]	90.0	90.0
SiC_2	P6/mmm	2.471	2.471	7.410	90.0	120.0

3.3 Electronic properties

The electronic structure of SiC_2 was examined using DFT to assess its suitability as an anode material. The total density of states (TDOS), shown in Figure 4, represents the overall state contributions from each atom in the structure and was further resolved through the partial

density of states (PDOS). Both silicon and SiC_2 exhibit state contributions in the valence band (VB) and conduction band (CB). The PDOS indicates that the dominant contributions arise from the p-orbitals of silicon and carbon, reflecting strong orbital hybridization between the two elements. SiC_2 displays a pseudo band gap near the Fermi level, characterized by reduced but nonzero states, implying that it is not a perfect semiconductor. Instead, it exhibits metallic characteristics, enhancing its conductivity. The valence band contains more pronounced peaks than the conduction band, suggesting that conductivity improves as electrons are thermally excited into the CB.

The electronic band structures of silicon and SiC_2, presented in Figure 5, further confirm metallic behavior. This is evidenced by multiple bands intersecting the Fermi level, with no distinct band gap along the Fermi line. The silicon phase considered here was metallic, and the incorporation of carbon enhances and sustains its electrical conductivity, while also supporting high charge carrier mobility—attributes favorable for anode performance.

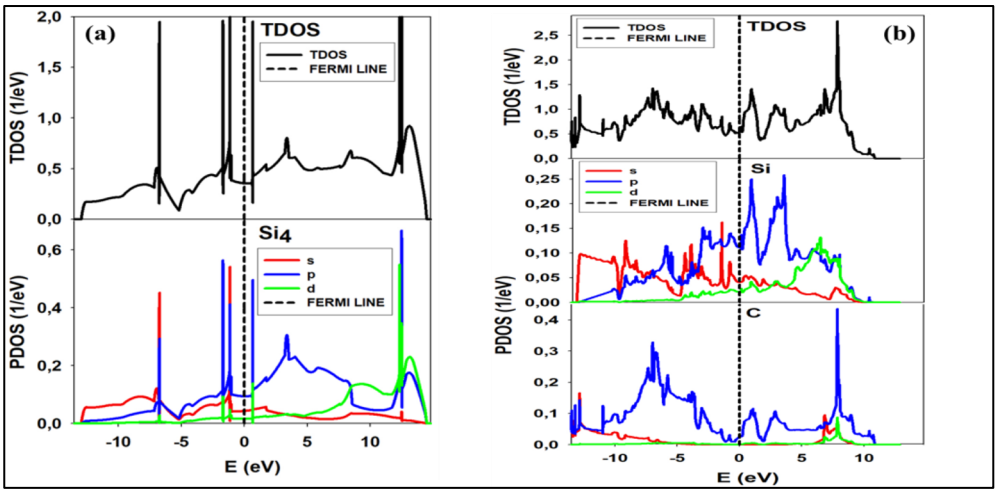

Fig. 4. The total density and partial density of states of (a) Si_4 and (b) SiC_2.

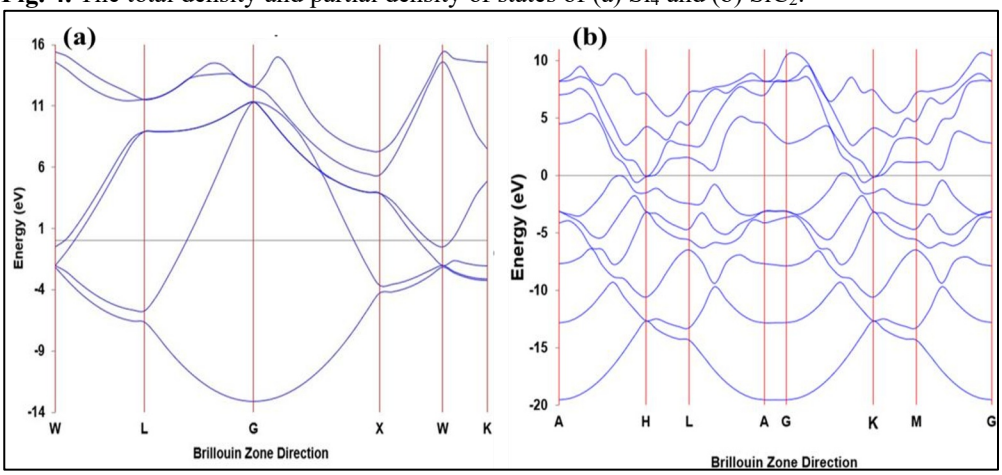

Fig. 5. Electronic band structure of (a) Si_4 and (b) SiC_2.

3.4 Mechanical properties

The elastic constants describe how a material responds to stress and strain along different directions, depending on its symmetry. They are crucial for evaluating both the mechanical stability and stiffness of materials. According to the Born stability criteria, a material is considered mechanically stable only if certain conditions are satisfied. Table 2 lists the elastic constants and moduli for Si and SiC_2, which possess cubic and hexagonal symmetries, respectively.

For cubic crystals, three independent elastic constants (C_{11}, C_{12}, C_{44}) define the stiffness matrix, and mechanical stability requires the following conditions:

$$C_{11} - C_{12} > 0,\ C_{11} + 2C_{12} > 0,\ C_{44} > 0$$

The Si structure fails to meet these requirements, indicating mechanical instability. Furthermore, with a Pugh's ratio below 1.75, it is classified as brittle.

For hexagonal crystals, five independent elastic constants (C_{11}, C_{12}, C_{13}, C_{33}, C_{44}) determine stability, with the following conditions to be satisfied:

$$C_{11}, C_{33}, C_{44} > 0,\ C_{11} - C_{12} > 0,\ C_{11} + C_{12} > 0,\ C_{33} + 2C_{13} > 0$$

The SiC_2 structure is mechanically unstable because C_{44} is negative. It also exhibits brittleness, as indicated by its Pugh's ratio being below 1.75.

Although both Si and SiC_2 are mechanically unstable and brittle, SiC_2 shows higher bulk, shear, and Young's moduli, suggesting greater resistance to compression, higher rigidity, and increased stiffness compared to pure Si.

Table 2. Elastic constants and the Bulk (B), Shear (G), Young's (E) moduli and Pugh's ratio ($\frac{B}{G}$) for Si and SiC_2.

Elasticity	**Si**	**SiC_2**
C_{11}	87.35	704.37
C_{12}	53.37	128.48
C_{13}	-	3.08
C_{33}	-	96.66
C_{44}	-15.30	-0.77
B	64.70	148.67
G	-33.11	197.19
E	-146.32	356.43
($\frac{B}{G}$)	-1.95	1.33

4 Conclusion

The cluster expansion method successfully generated eighteen thermodynamically stable carbon-doped silicon structures across four iterations, achieving high predictive accuracy with a low cross-validation score of 4.2 meV/atom. Among these, the SiC_2 phase was identified as the most stable, crystallizing in hexagonal symmetry that suggests a layered arrangement of closely packed atoms. This configuration enhances structural stability and yields superior mechanical properties compared to pure silicon. In particular, SiC_2 exhibits higher bulk, shear, and Young's moduli, indicating greater stiffness and resistance to compression despite its intrinsic brittleness.

Electronic structure analysis further reveals that SiC_2 displays metallic behavior, characterized by a pseudo band gap near the Fermi level and dominant contributions from the p-orbitals of silicon and carbon. The elevated density of states in the conduction band points to improved electrical conductivity. Overall, SiC_2 combines thermodynamic stability,

enhanced mechanical performance, and metallic conductivity, highlighting its potential as a promising anode material for future energy storage applications.

We sincerely acknowledge the National Research Foundation (NRF) for their financial support. This study utilized the computational resources of the Materials Modelling Centre (MMC) at the University of Limpopo and the Centre for High Performance Computing (CHPC) in Cape Town, South Africa.

Funding is provided by the National research foundation.

The data reported in this paper is available upon request to the corresponding author.

References

1. Y. Li, Q. Li, J. Chai, Y. Wang, J. Du, Si-based Anode Lithium-Ion Batteries: A Comprehensive Review of Recent Progress. ACS Mater. Lett. **5**, 2948–2970 (2023). https://doi.org/10.1021/acsmaterialslett.3c00253.
2. P.U. Nzereogu, A. D. Omah, F. I. Ezema, E. I. Iwuoha, A. C. Nwanya, Anode materials for lithium-ion batteries: A review. Appl. Surf. Sci. Adv. **9**, 100233 (2022). https://doi.org/10.1016/j.apsadv.2022.100233.
3. F.Z. Zhang, Y. Y. Ma, M. M. Jiang, W. Luo, J. P. Yang, Boron heteroatom-doped silicon–carbon peanut-like composites enables long life lithium-ion batteries. Rare Met. **41**, 1276–1283 (2022). https://doi.org/10.1007/s12598-021-01741-0.
4. R. Shao, F. Zhu, Z. Cao, Z. Zhang, M. Dou, Heteroatom-doped carbon networks enabling robust and flexible silicon anodes for high energy Li-ion batteries. J. Mater. Chem. A. **8**, 18338–18347 (2020). https://doi.org/10.1039/D0TA06647H.
5. B. Kim, J. Ahn, Y. Oh, J. Tan, D. Lee, J. K. Lee, J. Moon, Highly porous carbon-coated silicon nanoparticles with canyon-like surfaces as a high-performance anode material for Li-ion batterieS, J. Mater. Chem. A. **6**, 3028-3037 (2018). https://doi.org/10.1039/C7TA10093K.
6. X. Gao, W. Lu, J. Xu, Unlocking multiphysics design guidelines on Si/C composite nanostructures for high-energy-density and robust lithium-ion battery anode. Nano Energy, **81**, 105591 (2021). https://doi.org/10.1016/j.nanoen.2020.105591.
7. N. M. Saidi, M. A. Abdah, M. N. Mustafa, R. Walvekar, M. Khalid, A. Khosla, Advancements in Silicon Anodes for Enhanced Lithium-Ion Batteries Performance: Innovations Toward Next-Gen Superbatteries. Battery Energy, e20240048 (2025). https://doi.org/10.1002/bte2.20240048.
8. M. Wu, G. Cai, Z. Li, L. Ye, C. Wang, Structures and properties of carbon-doped silicon as anode material for lithium ions battery: A first-principles study. Vacuum, **225**, 113222 (2024). https://doi.org/10.1016/j.vacuum.2024.113222.
9. Q. Wu, B. He, T. Song, J. Gao, S. Shi, Cluster expansion method and its application in computational materials science. Comput. Mater. Sci. **125**, 243–254 (2016). https://doi.org/10.1016/j.commatsci.2016.08.034.
10. J. Hafner, Ab-initio simulations of materials using VASP: Density-functional theory and beyond. J. Comput. Chem. **29**, 2044–2078 (2008). https://doi.org/10.1002/jcc.21057.
11. W. Kohn, L. J. Sham, Self-Consistent Equations Including Exchange and Correlation Effects. Phys. Rev. **140**, A1133 (1965). https://doi.org/10.1103/PhysRev.140.A1133.

12. J. P. Perdew, K. Burke, M. Ernzerhof, Generalized Gradient Approximation Made Simple. Phys. Rev. Lett. **77**, 3865 (1996). https://doi.org/10.1103/PhysRevLett.77.3865.
13. H. J. Monkhorst, J. D. Pack, Special points for Brillouin-zone integrations. Phys. Rev. B. **13**, 5188-5192 (1976). https://doi.org/10.1103/PhysRevB.13.5188.
14. S. M. Jarkov, Y. N. Titarenko, G. N. Churilov, Electron microscopy studies of FCC carbon particles. Carbon, **36**, 595-597 (1998). https://doi.org/10.1016/S0008-6223(98)00072-4.
15. R. G. Diale, R. Modiba, P. E. Ngoepe, and H. R. Chauke, Phase stability of $TiPd_{1-x}Ru_x$ and $Ti_{1-x}PdRu_x$ shape memory alloys. Mater. Today: Proc. **38**, 1071-1076, (2021). https://doi.org/10.1016/j.matpr.2020.05.806.
16. S. J. Duclos, Y. K. Vohra, A. L. Ruoff, hcp to fcc transition in silicon at 78 GPa and studies to 100 GPa. Phys. Rev. Lett. **58**, 775-777 (1987). https://doi.org/10.1103/PhysRevLett.58.775.
17. D. C. Gleason-Rohrer, B. S. Brunschwig, N. S. Lewis, Measurement of the Band Bending and Surface Dipole at Chemically Functionalized Si(111)/Vacuum Interfaces. J. Phys. Chem. C. **117**, 18031-18042 (2013). https://doi.org/10.1021/jp401585s.